contribution to the XVIII ISPRS Congress Vienna 1996
International Archives for Photogrammetry and Remote Sensing, Volume XXXI, Part B, Commission VII

IN SITU BRDF MEASUREMENTS OF SELECTED SURFACE MATERIALS TO IMPROVE ANALYSIS OF REMOTELY SENSED MULTISPECTRAL IMAGERY

Gerhard Meister, Rafael Wiemker, Johann Bienlein, Hartwig Spitzer
II. Institut für Experimentalphysik
Universität Hamburg
Germany
Mail: G. Meister / KOGS, Vogt-Kölln-Str. 30, 22527 Hamburg, FRG
WWW-Page: http://kogs25.informatik.uni-hamburg.de/projects/censis/remotesens.html
E-mail: meister@kogs.informatik.uni-hamburg.de
Commission VII, Working Group 1

KEY WORDS: Radiometry, Multispectral, Infrared, Surface, Classification, Radiometric Measurement, BRDF Measurement, Spectralon BRDF

ABSTRACT

The spectral bidirectional reflectance distribution function (BRDF) of selected artificial surfaces (e. g. roof materials) was measured under natural illumination. Data were obtained with a spectrometer in the wavelength range 600 nm – 900 nm with a spectral resolution of 5 nm, using 61 spectral bands. The samples were placed on a goniometer, which allowed to set all the desired angles of incidence and reflection. A Spectralon panel (made by Labsphere Inc., Boulder, Colorado) was used as a reference target for determining the incoming irradiance. The BRDF of this Spectralon panel was measured in the laboratory. The BRDF of the Spectralon panel is not Lambertian, however it obeys Helmholtz's theorem of reciprocity. For the in situ measurements, an additional measurement was made for each combination of angles with the samples being shadowed, in order to determine the contribution of sky light. The samples could be fitted to a function which was developed by [Walthall, 1985] and modified by [Liang, 1994]. In this work, the function was extended by a specular peak, increasing the number of free parameters to 7. The diffuse part of the BRDF of the samples does not vary in a systematic way. The intensity of the specular peak grows with increasing zenith angles.

KURZFASSUNG

Dieser Beitrag beschäftigt sich mit der Messung der winkelabhängigen, spektralen Reflexionsfunktion (BRDF) von einigen ausgewählten künstlichen Oberflächen (z. B. Dachbedeckungen)bei natürlicher Beleuchtung. Als Meßgerät diente ein Spektrometer, welches im Bereich 600 nm – 900 nm Messungen in 61 Kanälen mit einer spektralen Auflösung von 5 nm ermöglicht. Die Proben wurden auf einem Goniometermeßtisch plaziert, so daß alle gewünschten Ein– und Ausfallswinkel eingestellt werden konnten. Zur Bestimmung der einfallenden Strahlungsflußdichte diente ein Reflektanznormal (Spectralon, hergestellt duch Labsphere Inc., Boulder, Colorado) als Referenzfläche, dessen BRDF zuvor im Labor bestimmt wurde. Es ergibt sich, daß die BRDF des Spectralons nicht dem Lambertstrahler entspricht, wohl aber dem Helmholtzschen Reziprozitätstheorem genügt. Bei den Feldmessungen wurde zusätzlich für jede Winkelkombination eine Messung bei beschatteter Probe durchgeführt, um den Einfluß des Himmelslichts zu bestimmen. An die Proben konnte eine Funktion angepaßt werden, die von [Walthall, 1985] entwickelt, von [Liang, 1994] modifiziert und hier um einen Term zur Modellierung des gespiegelten Anteils erweitert wurde, so daß diese Funktion insgesamt 7 freie Parameter besitzt. Während die diffuse Komponente der BRDF der Proben keine Systematik erkennen läßt, konnte bei der gespiegelten Komponente ein Anstieg der Intensität mit großen Zenitwinkeln festgestellt werden.

1 INTRODUCTION

The Bidirectional Reflectance Distribution Function (BRDF) as defined by [Nicodemus, 1970] describes the radiance emitted by a reflecting target into the sensor direction, depending on the incoming radiation, the angles of incidence and reflection $(\theta_i, \Phi_i, \theta_r, \Phi_r)$ (see fig.1) and wavelength λ.

The knowledge of the BRDF of surface materials is certainly crucial for proper analysis and evaluation of remotely sensed multispectral imagery. Spectral signatures change with viewing and illumination geometry, and the BRDF is thus needed for correct classification and change detection.

However, so far most multispectral image processing and classification is based on the simplifying assumption of Lambertian reflection, and thus prone to error. One of the reasons for this may be that only relatively few BRDF data are available, due to the tremendous effort necessary for its measurement. The work described here is aimed at measuring relevant BRDF data, finding proper BRDF models with few parameters, and thus finally improving classification of remotely sensed multispectral imagery.

In the line of our research we are interested in the use of multispectral imagery of high spatial resolution for purposes of urban planning and treaty verification in the framework of Open Skies. Most BRDF related efforts undertaken so far have been directed at natural surfaces such as vegetation and soils. In contrast to that we have chosen samples of artificial materials found in urban areas and man made structures such as tiles, bricks, asphalt, metall, roof materials etc., and measured their reflective behavior under natural illumintion.

2 EXPERIMENTAL SETUP

The measurements were done with the spectrometer OVID (Optical Visible and Infrared Detector) in cooperation with

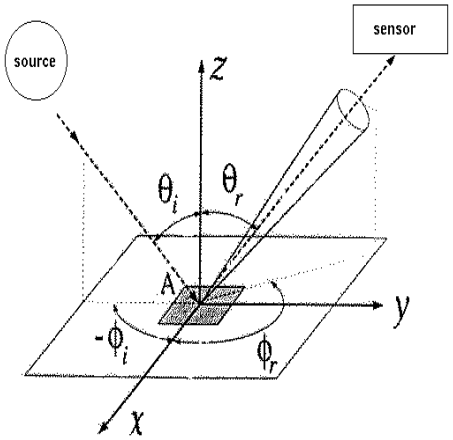

Figure 1: Definition of the angles
A denotes the surface of the sample

Max-Planck-Institut für Meteorologie, Hamburg, and Institut für Meteorologie, Universität Hamburg. A description of the sensor can be found in [Bartsch, 1994]. Each spectrum is recorded simultaneously for all wavelength bands by means of a CCD-Array. We used 61 spectral bands in the range $\lambda = 600 - 900$nm ($\Delta\lambda = 5$ nm), with a distance between sensor and samples of 1 m. The area on the sample covered by the instantaneous field of view (IFOV) of the sensor is about 10 cm^2.

A goniometer was constructed to hold the samples for all possible combinations of incidence and reflection angles. The goniometer allows to place the surface with arbitrary inclination towards sensor and light source (see [Meister, 1996]).

The samples were selected with respect to azimuthal symmetry, so that the BRDF's of the samples depend only on the azimuth difference angle $\nu = |\Phi_i - \Phi_r|$. We determined the BRDF of six samples: aluminum sprayed with red paint, a sheet of white smooth plastic, a concrete-type sidewalk cover block and three roof coverings (a red roofing tile, a slate-type tile and sprinkled roof paper). The values of the BRDF were measured at grid points of $0°, 25°, 50°, 75°$ for the zenith angles θ_i and θ_r respectively, and at $0°, 90°, 180°$ for the azimuth difference angle $\nu = |\phi_i - \phi_r|$,(see figure 1), making up a total of ca. 35 measured spectra for each sample.

As a reference target we used a commercially available Spectralon panel (Labsphere Inc., Boulder, Colorado) with an albedo of $\rho = 0.5$. Since we were not satisfied with the simplifying assumption of Lambertian behavior of the Spectralon panel, we adopted the following two step procedure (the second step was proposed by [Jackson, 1993]):

2.1 Step 1: Laboratory Measurement of the BRDF of the Spectralon Target

In the laboratory measurements, we used a 100 W halogene bulb as light source. We measured the reflected radiance L_r [W m^{-2}sr^{-1}nm^{-1}] from the Spectralon panel at the combinations of angles described above. Integrating L_r over the projected solid angle Ω as defined by [Nicodemus, 1970] and dividing the result by the albedo of the Spectralon yields the incident irradiance E_i [W m^{-2}nm^{-1}]:

$$E_i(\theta_i) = \frac{1}{\rho}\int L_r d\Omega =$$

$$\frac{1}{\rho}\int_{\nu=0}^{\nu=\pi}\int_{\theta_r=0}^{\theta_r=\frac{\pi}{2}} 2 \cdot L_r(\theta_i,\nu,\theta_r)\cos\theta_r \sin\theta_r d\theta_r d\nu \qquad (1)$$

These quantities allow to calculate the BRDF of the Spectralon :

$$f_r^{Spectralon}(\theta_i,\nu,\theta_r) \equiv \frac{dL_r(\theta_i,\nu,\theta_r)}{dE_i(\theta_i)} \qquad (2)$$

For small aperture solid angles, the BRDF can be approximated by

$$f_r^{Spectralon}(\theta_i,\nu,\theta_r) \approx \frac{L_r(\theta_i,\nu,\theta_r)}{E_i(\theta_i)} \qquad (3)$$

The results agree qualitatively very well with earlier measurements of the BRDF of Spectralon panels with an albedo of 1.0 by [Flasse, 1993] and [Jackson, 1992]. The BRDF values decrease with large zenith angles. The Spectralon panels with an albedo of 0.5 have a specular peak, that does not exist for the Spectralon panels with an albedo of 1.0 . The intensity of the specular peak increases rapidly with large zenith angles (see figures 3 and 4).

Our measurements suggest, that the BRDF of Spectralon obeys Helmholtz's theorem of reciprocity, i. e. , exchanging incidence and reflection angles does not change the BRDF value:

$$f_r(\theta_i,\nu,\theta_r) = f_r(\theta_r,\nu,\theta_i) \qquad (4)$$

This equation was confirmed by the measurement of the BRDF at 2×11 different combinations of angles (θ_i,ν,θ_r). The BRDF of the Spectralon panel is presented in figures 3 and 4.

The wavelength dependence of the diffuse component and the specular component of the BRDF of the Spectralon panel is linear, see [Meister, 1996].

2.2 Step 2: Outdoor Measurement of the BRDF's of the selected surfaces

Four measurements of the reflected radiance $L_r(\lambda)$ are necessary in order to obtain the Bidirectional Reflectance Factors (BRF) of the samples for each combination of angles :

1. L_r of the Spectralon panel illuminated by the sun and skylight
2. L_r of the Spectralon panel illuminated by skylight only. To this aim, the Spectralon panel was cast in shadow. The contribution of diffuse skylight to the global irradiance was 20% on average, obviously depending strongly on the angle of incidence θ_i.

   The difference between these two measurements yields the radiance ΔL_r reflected by the Spectralon panel which can be attributed to direct sunlight only. The incoming radiance E_i^{sun} from the sun can be calculated from the BRDF of the Spectralon panel, determined in step 1:

$$E_i^{sun}(\theta_i) = \frac{f_r^{Spectralon}(\theta_i,\nu,\theta_r)}{\Delta L_r(\theta_i,\nu,\theta_r)} \qquad (5)$$

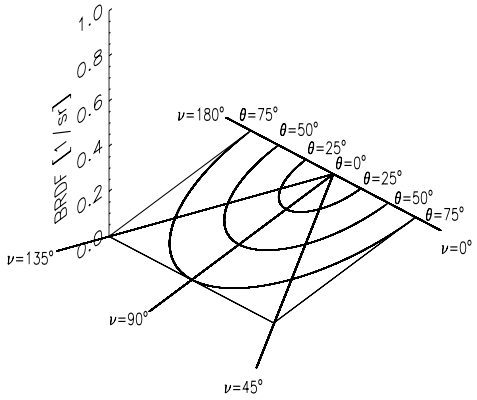

Figure 2: Legend of the 3-dimensional plots $\nu = |\phi_i - \phi_r| \bmod 180°$ (planar symmetry is assumed in fig. 3-10), $\theta = \theta_r$ (angles greater than $75°$ are not shown)

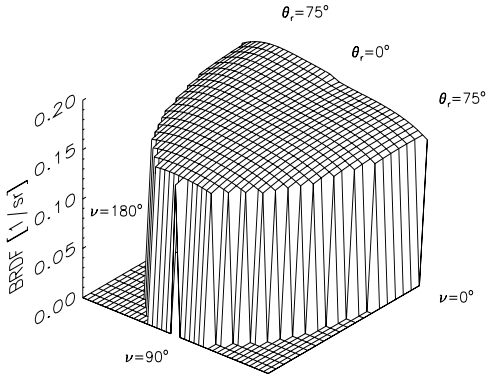

Figure 3: BRDF of the Spectralon panel at $\theta_i = 25°$ and $\lambda = 850$ nm

3. L_r of the sample illuminated by the sun and skylight
4. L_r of the sample illuminated by skylight only
   Here again, the difference between the last two measurements yields the radiance ΔL_r reflected by the sample which can be attributed to direct sunlight only. Assuming, that the incoming irradiance E_i^{sun} does not change between the two measurements, the value of the BRDF of the sample can then be obtained from

$$f_r^{sample}(\theta_i, \nu, \theta_r) = \frac{\Delta L_r(\theta_i, \nu, \theta_r)}{E_i^{sun}(\theta_i)} \qquad (6)$$

   Of course, the incoming irradiance E_i^{sun} did change between the two measurements. The difference (5.4% on average) was included into the calculation of the error.

The measurements were performed on the roof of a 20-storied building in the month of april at clear skies.

Aside from azimuthal symmetry, the samples should meet the following requirements, if the BRDF of the sample is to be measured with the above procedure:

- The BRDF of the sample must not change between the measurements. In our experiment, several days passed between the measurements, this excludes the determination of the BRDF of vegetation.

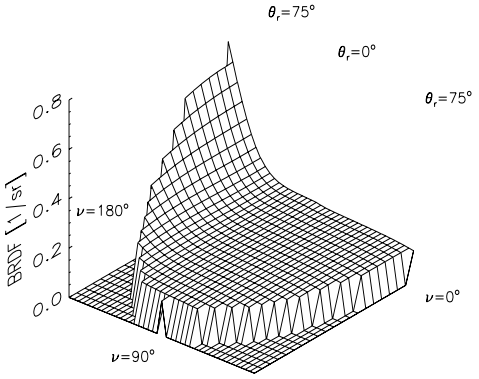

Figure 4: BRDF of the Spectralon panel at $\theta_i = 75°$ and $\lambda = 850$ nm

- If the diffuse component is very weak, the intensity of light emitted into a nonspecular direction differs hardly between the measurements 3 and 4 described above. Thus the difference between these measurements will be small and the relative error of ΔL_r will increase strongly. E.g., we did not succeed in fitting a BRDF-model to the data of a sample of aluminum and a sample of black roof paper, both of them have a negligible diffuse component.

3 BRDF-MODEL FITTING

Several BRDF-models (e.g. polynomials, spherical harmonics, and functions proposed by [Oren, 1995] and [Minnaert, 1941]) were fitted to the measured data points, using a least-squares-algorithm. The compatibility of the measured data and the fitted BRDF-models was judged by means of a χ^2-test. The best results were obtained with a model proposed by [Walthall, 1985]. This model was modified by [Liang, 1994] to be compatible with Helmholtz's theorem of reciprocity. We extended it by an additional Gaussian peak accounting for specular reflection:

$$f_r = a_0 + a_1 \cdot (\theta_i^2 + \theta_r^2) + a_2 \cdot (\theta_i^2 \cdot \theta_r^2) + a_3 \cdot (\theta_i \cdot \theta_r) \cdot \cos\nu + a_4 \cdot e^{a_5 \cdot (\theta_i \cdot \theta_r)^2} \cdot e^{-a_6 \cdot r^2} \qquad (7)$$

where the free parameters a_0 to a_3 describe Walthall's model, and the last 3 parameters are our extension for specular reflection with r being the angle between the reflected light (direction θ_r, ν) and the specular angle ($\theta_i, \nu = 180°$) (direction of the incident radiation: $\theta_i, \nu = 0°$). The term $e^{a_5 \cdot (\theta_i \cdot \theta_r)^2}$ models the increasing intensity of the specular peak with increasing zenith angles. For θ_i and θ_r fixed, the term $e^{-a_6 \cdot r^2}$ produces a Gaussian peak.

So the total number of free parameters of this model is 7, and thus well over-determined by the ca. 35 measured data points per sample and wavelength.

[Liang, 1994] also modeled the 'hot spot' (a peak reflected back into the direction of the light source). We did not include the 'hot spot' term, because our experimental setup prevented to measure at angles where the 'hot spot' occurs.

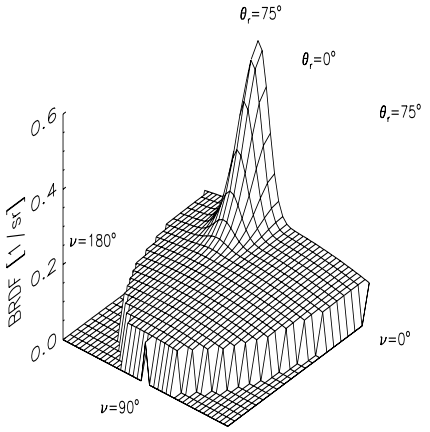

Figure 5: BRDF of the sample 'Sprayed aluminium' at $\theta_i = 25°$ and $\lambda = 850$ nm

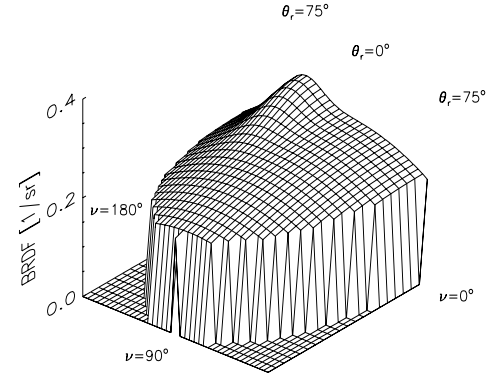

Figure 6: BRDF of the sample 'plastic' at $\theta_i = 25°$ and $\lambda = 850$ nm

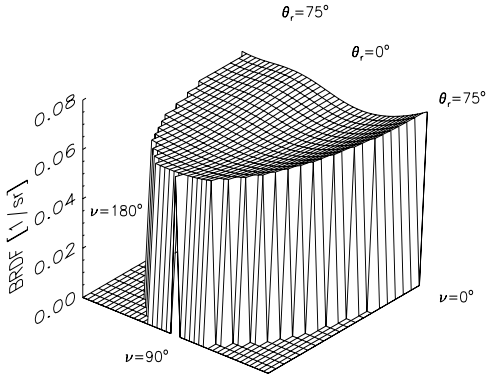

Figure 7: BRDF of the concrete panel at $\theta_i = 25°$ and $\lambda = 850$ nm

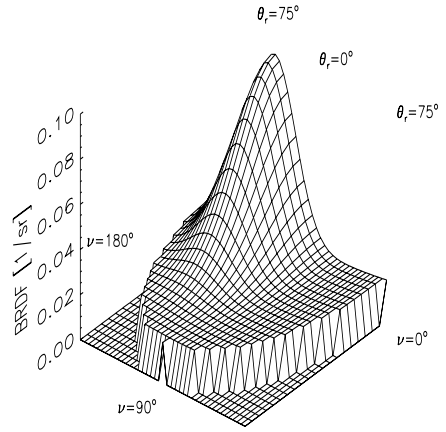

Figure 8: BRDF of the sample 'slate' at $\theta_i = 25°$ and $\lambda = 850$ nm

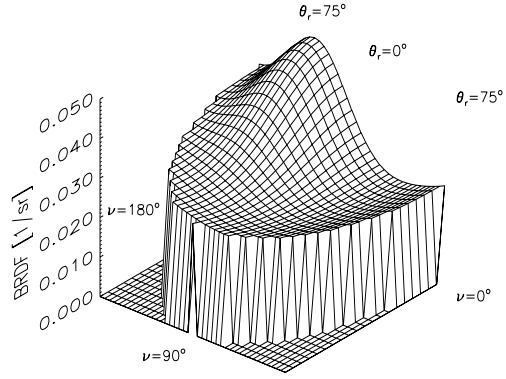

Figure 9: BRDF of the 'sprinkled wall paper' panel at $\theta_i = 25°$ and $\lambda = 850$ nm

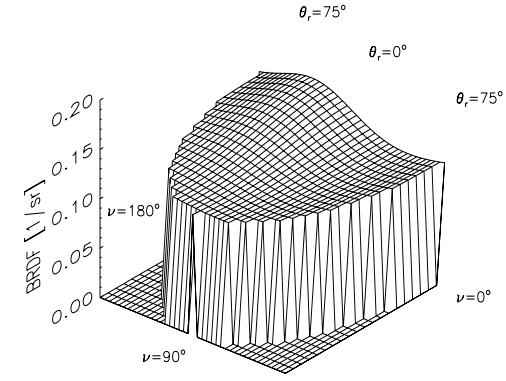

Figure 10: BRDF of the sample 'Roofing tile' at $\theta_i = 25°$ and $\lambda = 850$ nm

Neither Walthall's model nor our proposal to account for the specular peak are based on theoretical assumptions. f_r as defined in equation 7 is just an empirical function to describe the measured data.

4 RESULTS OF THE BRDF-MODEL-FITTING TO THE SELECTED SURFACE SAMPLES

Fig. 5-10 show the BRDF of the samples as fitted by equation 7. There was no uniform angular dependence of the samples. The BRDF of some of the samples increased with increasing zenith angles (e.g. concrete), whereas the BRDF of other samples decreased with increasing zenith angles (e.g. plastic). The variation due to the diffuse component is usually less than 15 % (not taking into account zenith angles greater than $75°$). The intensity of the specular peak dominates the visual impression of figures 5 to 10.

No simple rules could be deduced from the wavelength dependence of the coefficients a_0 to a_3, which describe the diffuse component. The wavelength dependence of the coefficients a_4 to a_6, which describe the specular component, is almost always linear or even constant.

The coefficients of the samples are given in tables $11-13$ at a wavelength of $\lambda = 650, 750, 850$ nm respectively. The error was calculated from the corresponding covariance matrix. The relative error of the fitted BRDF varies between 2 and 7%.

All the selected samples pass the χ^2 test. We conclude that the function of [Walthall, 1985] with the modifications of [Liang, 1994], extended by a specular peak, is best suited for describing the BRDF of the samples studied by us.

5 OUTLOOK

We plan to apply the here discussed experimental results to multispectral imagery recorded with the DAEDALUS AADS 1268 scanner. The imagery was acquired during several campaigns in cooperation with the German Aerospace Research Establishment (DLR) and is described in previous communications [Hepp, 1994].

ACKNOWLEDGEMENTS

Dr. Barbara Bartsch put the spectrometer OVID at our disposal. She and Dr. Martin Kollewe enabled us to carry out the measurements. We want to thank them for their contributions.

REFERENCES

[Walthall, 1985] C. L. Walthall and J. M. Norman and J. M. Welles and G. Campbell and B. L. Blad, 1985. Simple equation to approximate the bidirectional reflectance from vegetation canopies and bare soil surfaces, Applied Optics, 24, pp. 383-387.

[Liang, 1994] S. Liang and A. H. Strahler, 1994. Retrieval of Surface BRDF from Multiangle Remotely Sensed Data, Remote Sensing of Environment, 50, pp. 18-30.

[Nicodemus, 1970] F.E. Nicodemus, 1970. Reflectance Nomenclature and Directional Reflectance and Emissivity, Applied Optics, 9 (6), pp. 1474-1475.

[Bartsch, 1994] B. Bartsch and S. Bakan and J. Fischer, 1994. Remote Sensing of Water Vapour within the Solar Spectrum, SPIE (The International Society for Optical Engineering), 2311, pp. 197-206.

[Meister, 1996] G. Meister, 1996. Messung der spektralen Reflexionsfunktion (BRDF) ausgewählter Oberflächen bei natürlicher Beleuchtung, diploma thesis, Universität Hamburg, II. Institut für Experimentalphysik, CENSIS-REPORT-18-96.

[Jackson, 1993] Ray D. Jackson and Elizabeth A. Walter-Shea and Cynthia J. Hays and Mark A. Mesarch, 1993. An Improved Goniometer System for Calibrating Field Reference-Reflectance Panels, Remote Sensing of Environment, 43, pp. 131-138.

[Flasse, 1993] Stephane P. Flasse and Michel M. Verstraete and Bernard Pinty and Carol J. Bruegge, 1993. Modeling Spectralon's bidirectional reflectance for in-flight calibration of Earth-orbiting sensors, SPIE (The International Society for Optical Engineering), 1938, pp. 100-108.

[Jackson, 1992] R. D. Jackson and T. Clarke and S. Moran, 1992. Bidirectional Calibration Results for 11 Spectralon and 16 $BaSO_4$ Reference Reflectance Panels, Remote Sensing of Environment, 40, pp. 231-239.

[Oren, 1995] M. Oren and S.K. Nayar, 1995. Generalization of the Lambertian Model and Implications for Machine Vision, International Journal of Computer Vision, 14, pp. 227-251.

[Minnaert, 1941] M. Minnaert, 1941. The reciprocity principle in lunearphotometry, Astrophys. J., 93, pp. 403-410.

[Hepp, 1994] T. Hepp, 1994. Erzeugung multispektraler Reflektanzbilder zur automatisierten Bildauswertung, diploma thesis, Universität Hamburg, II. Institut für Experimentalphysik, CENSIS-REPORT-10-94.

	a_0 $[\mathrm{sr}^{-1}]$	a_1 $[\mathrm{sr}^{-1} \cdot \mathrm{rad}^{-4}]$	a_2 $[\mathrm{sr}^{-1} \cdot \mathrm{rad}^{-2}]$	a_3 $[\mathrm{sr}^{-1} \cdot \mathrm{rad}^{-2}]$	a_4 $[\mathrm{sr}^{-1}]$	a_5 $[\mathrm{rad}^{-4}]$	a_6 $[\mathrm{rad}^{-2}]$
Spectralon	0.153	-0.0260	0.0041	-0.0149	0.0178	1.15	1.11
Sprayed Aluminum	0.165	-0.0232	0.0157	-0.0130	0.42	1.50	21.73
Plastic	0.252	-0.0361	-0.0099	0.0073	0.0708	0.98	8.39
Concrete	0.053	0.0062	-0.0053	0.0094	0.0099	1.39	2.17
Slate	0.0149	0.0029	-0.0043	0.0001	0.0702	1.66	4.84
Sprinkled wall paper	0.0156	0.0053	-0.0018	-0.0054	0.0251	1.12	2.60
Roofing tile	0.078	0.0128	-0.0123	-0.0087	0.0364	1.14	2.07

Table 11: Coefficients of the BRDF of the samples

at $\lambda = 650$ nm (cf. equation 7)

	a_0 $[\mathrm{sr}^{-1}]$	a_1 $[\mathrm{sr}^{-1} \cdot \mathrm{rad}^{-4}]$	a_2 $[\mathrm{sr}^{-1} \cdot \mathrm{rad}^{-2}]$	a_3 $[\mathrm{sr}^{-1} \cdot \mathrm{rad}^{-2}]$	a_4 $[\mathrm{sr}^{-1}]$	a_5 $[\mathrm{rad}^{-4}]$	a_6 $[\mathrm{rad}^{-2}]$
Spectralon	0.154	-0.0246	0.0039	-0.0147	0.0184	1.15	1.08
Sprayed Aluminum	0.163	-0.0232	0.0154	-0.0115	0.43	1.55	22.0
Plastic	0.271	-0.0391	-0.0122	0.0146	0.0629	1.01	8.07
Concrete	0.053	0.0065	-0.0060	0.0087	0.0088	1.47	2.17
Slate	0.0164	0.0020	-0.0037	0.0009	0.0708	1.70	4.88
Sprinkled wall paper	0.0176	0.0050	-0.0016	-0.0063	0.0239	1.17	2.93
Roofing tile	0.110	0.0109	-0.0213	0.0014	0.0394	1.15	1.81

Table 12: Coefficients of the BRDF of the samples

at $\lambda = 750$ nm (cf. equation 7)

	a_0 $[\mathrm{sr}^{-1}]$	a_1 $[\mathrm{sr}^{-1} \cdot \mathrm{rad}^{-4}]$	a_2 $[\mathrm{sr}^{-1} \cdot \mathrm{rad}^{-2}]$	a_3 $[\mathrm{sr}^{-1} \cdot \mathrm{rad}^{-2}]$	a_4 $[\mathrm{sr}^{-1}]$	a_5 $[\mathrm{rad}^{-4}]$	a_6 $[\mathrm{rad}^{-2}]$
Spectralon	0.154	-0.023	0.0037	-0.0145	0.019	1.15	1.06
Sprayed Aluminum	0.138	-0.0184	0.0158	-0.0136	0.43	1.56	22.1
Plastic	0.273	-0.0389	-0.0121	0.0166	0.0564	1.03	7.98
Concrete	0.052	0.0072	-0.0066	0.0077	0.0087	1.50	2.22
Slate	0.0138	0.0029	-0.0040	0.0001	0.0725	1.67	4.91
Sprinkled wall paper	0.0190	0.0050	-0.0015	-0.0072	0.0241	1.17	3.06
Roofing tile	0.104	0.0117	-0.0191	-0.0018	0.0395	1.16	1.88

Table 13: Coefficients of the BRDF of the samples

at $\lambda = 850$ nm (cf. equation 7)